

## 13.3 Correcting for Position Errors in Variational Data Assimilation

THOMAS NEHRKORN, BRYAN WOODS, ROSS N. HOFFMAN

*Atmospheric and Environmental Research, Inc., Lexington, MA*

AND THOMAS AULIGNÉ

*National Center for Atmospheric Research, Boulder, CO*

### ABSTRACT

The Feature Calibration and Alignment technique (FCA) has been developed to characterize errors that a human would ascribe to a change in the position or intensity of a feature, such as a hurricane. Here FCA is implemented in the Weather Research and Forecasting Data Assimilation system (WRFDA) to correct position errors in background fields and tested in simulation for the case of Hurricane Katrina (2005). Within data assimilation, FCA can be used to explain part of the background error in terms of displacement vectors and make the residual background errors smaller and more nearly Gaussian. Here, FCA determines a set of 2d displacement vectors to improve the alignment of features in the forecast and observations by solving the usual WRFDA variational data assimilation problem—simultaneously minimizing the misfit to observations and a constraint on the displacements. This latter constraint is implemented by hijacking the usual WRFDA background term for the mid-level  $u$ - and  $v$ -wind components. The full model fields are then aligned using a procedure that minimizes dynamical imbalances by displacing only conserved or quasi-conserved quantities. Simulation experiments show the effectiveness of these procedures in correcting gross position errors and improving short-term forecasts. Compared to earlier experiments, even this initial WRFDA implementation produces improved short-term forecasts. Adding FCA to WRFDA advances FCA towards mainstream implementation since all observations with a corresponding WRFDA observation operator may be used for FCA and the WRFDA methodology for estimating the background error covariances may be used to refine the displacement error covariances.

---

### 1. Introduction

In meteorology and other geophysical fluid contexts it is often useful to characterize the flow in terms of features—a hurricane, the Gulf Stream, and so forth. In discussing differences between two estimates<sup>1</sup> of a feature, it is often useful to describe the differences in terms of the intensity and position of key features in the flow. Differences in the position of a feature especially result in errors with substantial and complex spatial correlations, that may also be non-Gaussian (Lawson and Hansen 2005). Such errors are certainly not captured by static error covariance models. For some variables (precipitation, chlorophyll concentration, ground-water variables) anamorphic transformations can reduce the non-Gaussianity of errors (*e.g.*, Simon and Bertino 2009; Schöniger et al. 2012). Such “Gaussian anamorphisms” can also increase the background error correlation radius which should im-

prove the data assimilation as this tends to increase the benefit from each observation (Brankart et al. 2012).

For data assimilation it is assumed that error statistics are Gaussian and known. Actual errors may be non-Gaussian and, at best, the error statistics are approximately known. Specifying the error statistics is itself an estimation exercise. With limited data available it is desirable to have parsimonious representation of these error statistics.<sup>2</sup> Errors caused by a feature being incorrectly positioned can be parsimoniously described in terms of displacements. This suggests solving for the displacements, anticipating that the residual errors after aligning the background field will be smaller and more nearly Gaussian. We have developed the Feature Calibration and Alignment technique (FCA) to solve this problem (Hoffman et al. 1995; Hoffman and Grassotti 1996;

---

<sup>1</sup>If one is taken to be the truth, then the differences are errors.

*Corresponding author address:* Thomas Nehrkorn, AER, 131 Hartwell Avenue, Lexington, MA 02421. E-mail: [tnehrkor@aer.com](mailto:tnehrkor@aer.com)

<sup>2</sup>For example, errors of a particular variable, say ocean surface wind speed, may vary with location and season in some complex way, while in fact the errors depend principally on wind speed magnitude itself and then on location and season through the variability of wind speed (Hoffman et al. 2013).

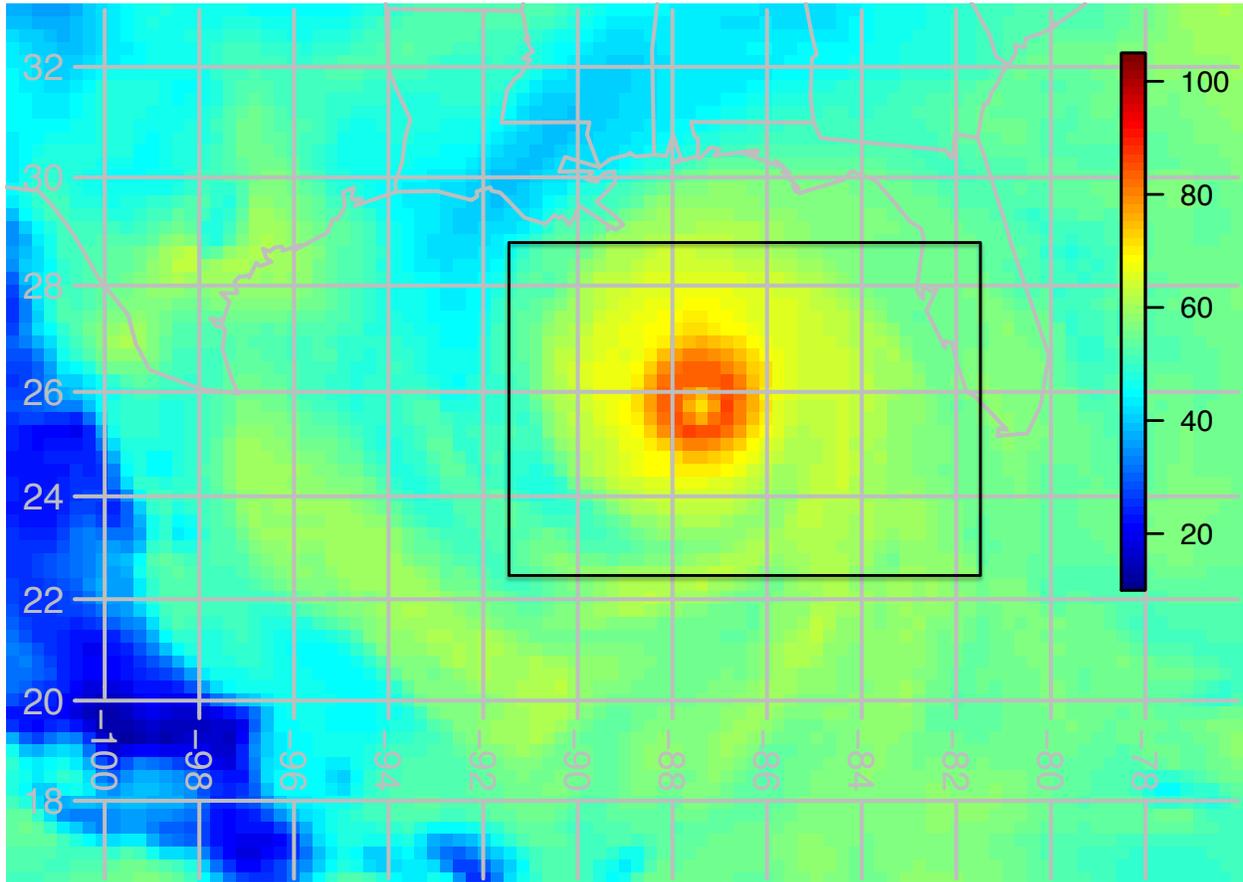


FIG. 1. Location of the study domain. A 30 km grid covering the area shown is used in all FCA calculations and for all WRF forecasts. Latitude north and longitude east and state boundaries are indicated in grey. IWV in  $\text{kg m}^{-2}$  is shown (in the same color scale used in subsequent figures) for the nature run simulation of Hurricane Katrina. All subsequent figures are for the area of the black box containing the IWV signature of Katrina.

Grassotti et al. 1999; Nehr Korn et al. 2003, 2014). In this study FCA is used to correct position errors in background fields. To do this, FCA determines 2d displacement vectors by solving the usual WRFDA variational data assimilation problem, but with the displacements as the control vector. Nehr Korn et al. (2014) generalized the method of Hsiao et al. (2010) to apply horizontal displacements to 3d model fields without introducing large imbalances, and this method is used here. Many additional studies (Ahijevych et al. 2009, and references therein) have taken a feature oriented approach for verification and sometimes data assimilation. For example, Beezley and Mandel (2008) makes use of “morphing”.<sup>3</sup>

<sup>3</sup>FCA can operate on images in a similar way, but we have developed FCA so that it can also use any type of data to align a background state.

Additional examples of feature alignment in data assimilation are given by Nehr Korn et al. (2014).

In the present paper, we report on a major step towards operationalizing FCA. This work extends similar experiments reported by Nehr Korn et al. (2014), but in the earlier work we used IWV observations alone to determine the alignment using the approach of Grassotti et al. (1999). Now, FCA is integrated into the WRFDA (Barker et al. 2012) (see Section 3) and (pseudo-)radiosonde observations were used to determine the alignment. In an idealized experiment for Hurricane Katrina (2005) (Section 2) we demonstrate how FCA corrects gross position errors and how FCA alone improves short-term forecasts, and that using radiosonde observations results in greater improvement compared to IWV observations (Section 4). FCA in WRFDA is a key advance since all

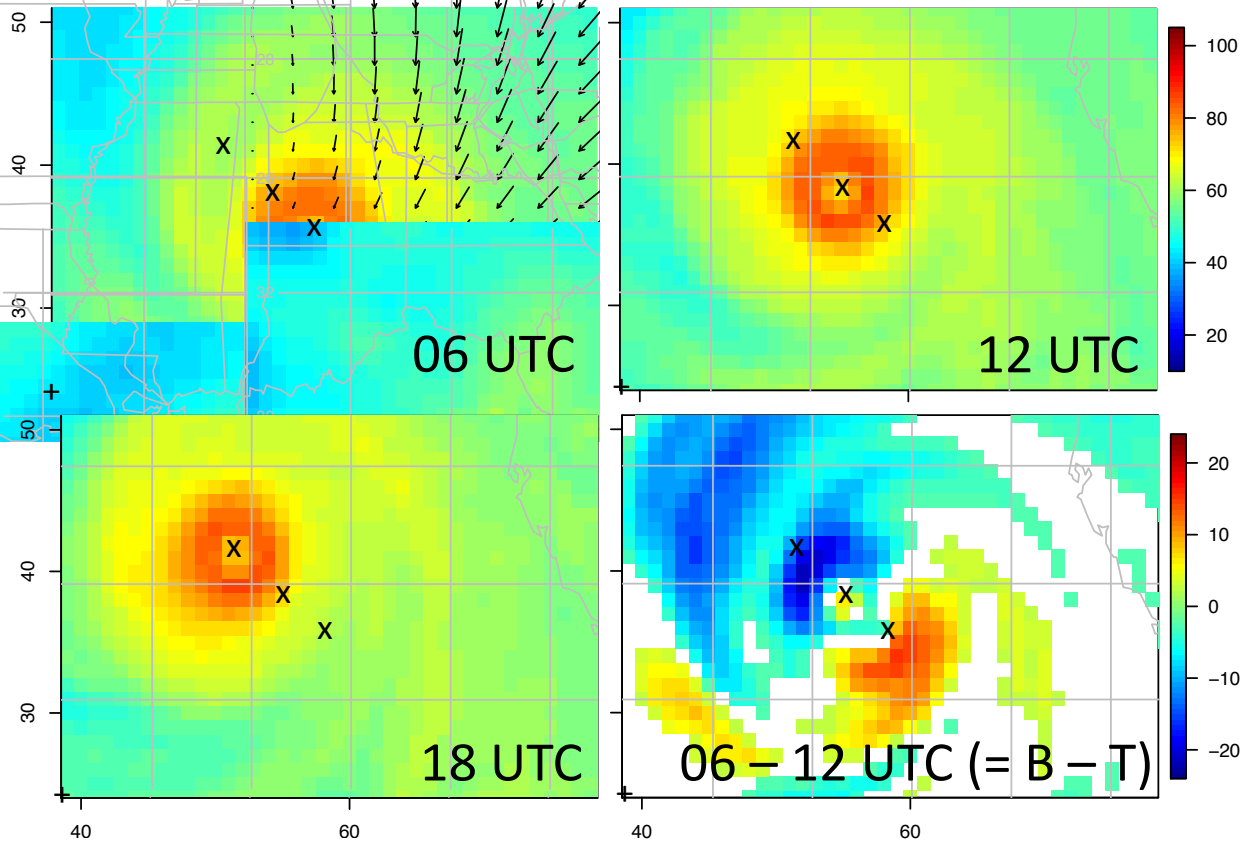


FIG. 2. IWV in  $\text{kg m}^{-2}$  for the nature run at 06, 12, and 18 UTC and the difference of 06–12 UTC. Roughly speaking, the IWV signature of Katrina is tracking steadily to the NW. The color scales shown are used on all figures. The three “X” marks on each panel (and on the panels of all subsequent figures) indicate the centers of the IWV feature at the three synoptic times shown.

observations with a corresponding WRFDA observation operator may be used for FCA and the WRFDA methodology for estimating the background error covariances may be used to refine the displacement error covariances (Section 5).

## 2. Simulation experiments

Identical twin Observing System Simulation Experiment (OSSE) for Hurricane Katrina (2005) are used here and by Nehrkorn et al. (2014) to test the utility of FCA-derived displacements to align 3d model fields. The default WRF tutorial Katrina case, run for 24 hours from 00 UTC 28 August 2005, provides the nature run (NR). The model domain is shown in Fig. 1. For this NR, Global Forecast System (GFS) analyses provide the initial and boundary conditions; grid spacing is 30 km; there are 28 levels; and the time step is 180 s. The NR at 06 UTC is

then taken to be the background or first guess for the 12 UTC analysis. That is, the NR at 12 UTC is the truth. Observations are constructed by spatially subsampling the NR at 12 UTC every third grid point in each direction, excluding a 5-grid point border, to create a set of simulated observations. This provides FCA with a set of observations that are synoptically consistent with the truth (NR at 12 UTC) and a background showing the hurricane displaced to the southeast. The FCA-determined displacements are used to align the 3d background fields and then short-term forecasts are run from 12 UTC to 18 UTC.

Figure 2 shows the evolution of IWV in the NR and the IWV background error. Over this period, Katrina moves steadily towards the NW. Consequently there is a significant dipole error structure consistent with this movement—the background IWV is low in the area of

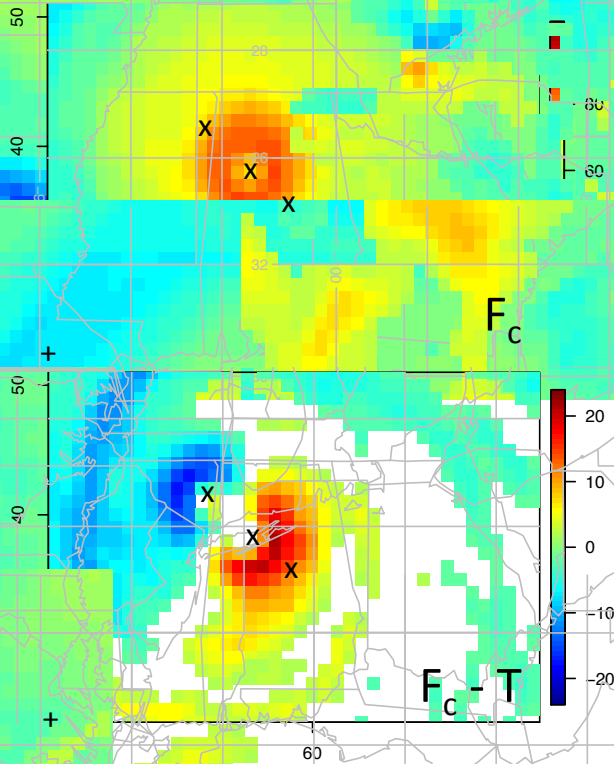


FIG. 3. The IWV control forecast and forecast error at 18 UTC. The WRF forecast model, even at the coarse 30 km resolution used, is able to correctly capture the movement of the IWV signature of Katrina. Therefore the control forecast beginning with IC that lags the nature run by 6 h, continues to lag the nature run by 6 h and the forecast error is very similar in structure to the initial error (panel labeled B–T in Fig. 2) but shifted towards the NW.

the true storm location and high in the area of the storm location in the background. Basic statistics for the error in the region plotted, as well as for all other difference fields plotted, are given in Table 1. Figure 3 shows the control forecast valid at 18 UTC. Since the control forecast basically started from the NR model state that was 6 hours old, it continues to lag the truth by 6 hours and position Katrina in the forecast valid at 18 UTC, close to the true location at 12 UTC. The forecast error structure of control is similar to the initial condition error structure but shifted to the NW. So the forecast error is similar to the difference of truth at 12 UTC and 18 UTC. Similarly the control forecast initial conditions are equal to the truth at 06 UTC and the initial conditions error is the difference of truth at 06 UTC and 12 UTC. Finally,

TABLE 1. IWV error statistics ( $\text{kg m}^{-2}$ ). The first group (the background and analyses) are calculated from fields valid at 12 UTC and the second group (the forecasts) are calculated from fields valid at 18 UTC.

Error	Fig.	Mean	s.d.	RMS	Min.	Max.
B–T	2	-2.22	6.37	6.75	-21.35	15.73
A–T	7	-0.12	3.93	3.93	-17.16	20.09
$A^{IWV}$ –O	10	-0.63	2.56	2.64	-7.62	7.83
$A^{IC}$ –T	11	0.24	4.22	4.23	-26.28	21.03
$F_c$ –T	3	-0.92	5.56	5.64	-17.34	21.30
$F_a$ –T	8	0.07	2.90	2.90	-6.65	8.31
$F_a^{IC}$ –T	12	0.15	3.56	3.57	-15.24	14.19

since the core of Katrina in the NR is basically tracking steadily towards the NW, these two difference fields are very similar in structure, but shifted along the storm track.

### 3. Formulation of FCA for WRFDA

First guess fields used in data assimilation procedures, typically short-term forecasts, often contain errors caused by position errors of coherent structures or features. FCA provides an alternative to correcting the first guess with additive increments by explicitly correcting position errors.

Nehrkorn et al. (2014) implemented FCA as a standalone preprocessor to WRF using the methodology of Grassotti et al. (1999). Now we have implemented a prototype FCA algorithm directly into the quasi-operational WRF variational data assimilation system (DAS), providing a seamless integration with the rest of the WRF functionality. In the WRF DAS (hereafter WRFDA) prototype we define the cost function  $J = J_b + J_o$ . The usual definitions of  $J_b = (x - x_b)^T B^{-1} (x - x_b)$  and  $J_o = (y - H(x))^T R^{-1} (y - H(x))$  are used, but with some critical modifications. Here, the observation vector  $y$  is unchanged from normal usage, but now the control vector  $x$  contains only the eastward- and northward-components of the displacement field. Likewise the observation error covariance matrix  $R$  (taken to be the identity matrix here) is unchanged from normal usage, but now the background error covariance matrix  $B$  is defined below in Section 3.b to be appropriate for the displacements. In this study,  $x_b = 0$ , *i.e.*, the prior for the displacements is zero. The observation operator  $H = H(x; z_b)$  may be considered to have two steps: First, use the current estimate of the displacements  $x$  to align the (constant) prior model state, here de-

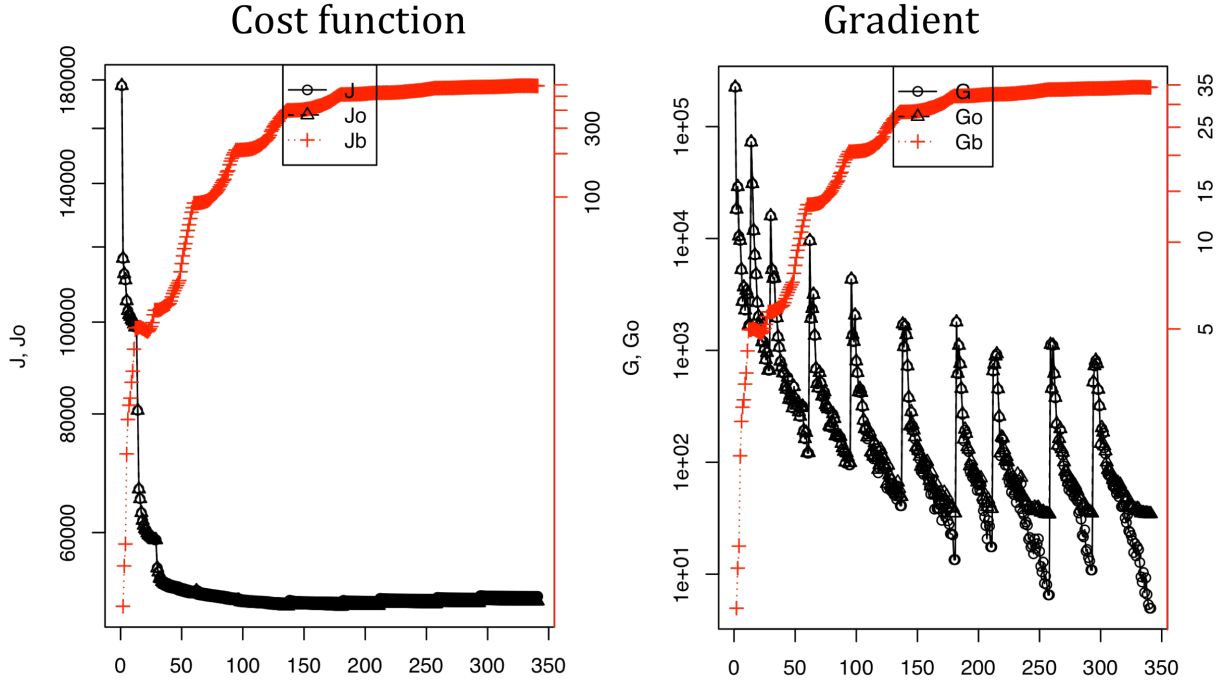


FIG. 4. Cost function (left) and gradient (right) for the WRFDA FCA calculation of the Hurricane Katrina case for ten outer loop steps (OLSs). Values for the total and observation cost function are shown in black (left axis), and those for the background are shown in red (right axis). Notice the difference in scale. Both y-axes are logarithmic. The x-axis is labeled by the cumulative inner iteration number.

noted  $z_b$ .<sup>4</sup> Second, apply the usual observation operator to the result of the first step. In the first step, the model fields are aligned using the Nehr Korn et al. (2014) generalization of the method of Hsiao et al. (2010). Details are in Nehr Korn et al. (2014), but in brief: Wind components ( $u$ ,  $v$ ,  $w$ ), sea level pressure, relative humidity and hydrometeor mixing ratios are all displaced along model surface and potential temperature is displaced along constant height surfaces. Then pressure, specific humidity, temperature, hydrostatic geopotential and dry air mass are calculated. Nonhydrostatic geopotential is not displaced. Since only conserved or quasi-conserved quantities are displaced, these steps aim to limit imbalances in the aligned fields.

Integration in the WRF DAS (hereafter WRFDA) allows for the reuse of multiple software, including: minimization, control vector transformation, observation ingest, user interface, file input/output (I/O), and visualization. For example, Grassotti et al. (1999) used the Gay

<sup>4</sup>Usually the prior model state is denoted  $x_b$ , but in this prototype implementation of FCA in WRFDA, the model state is not part of the control vector.

(1990) nonlinear minimization. This has now been replaced with the conjugate gradient minimization within WRFDA. The re-use of the observation ingest alone eliminates the need to redevelop separate quality control and observation operator software, and makes it possible to use all of the observation types supported by WRFDA.

The WRFDA integration of FCA results in several improvements. Grassotti et al. (1999) constrained the displacements using a penalty function comprised of terms designed to ensure smoothness, non-divergence, reasonable physical magnitudes, etc. and used a truncated spectral representation for the displacement vector. In contrast, the WRFDA implementation leverages the existing control vector, model coordinate space, and background error representation of Wu et al. (2002) and Michel and Auligné (2010). In the WRFDA FCA prototype described here, the background error covariances derived for the wind field increments are used to constrain the displacement vector, and the existing WRFDA mechanisms allow adjusting error magnitudes and correlation length scales. This provides improved consistency and tighter coupling between the minimization and adjustment of the model

fields: displacement vectors are derived for an optimal fit of the displaced model fields to the available observations, rather than applying displacement vectors to model fields after their offline derivation using 2d derived fields. The application of the displacements inside of the DAS provides a natural path for developing an algorithm that allows displacements to vary with height and/or allows for 3d displacements.

#### *a. WRFDA displacement implementation*

To maximize re-use of existing WRFDA software, the displacement vectors make use of the storage allocated for the  $u$ - and  $v$ -components of the wind increment during the control vector transformation. (Note that to enable simultaneous optimization of displacement and additive analysis increments, the current prototype implementation would need to be modified to allocate separate storage for the displacement vectors, and to concatenate these with the normal WRFDA control vector.) During the forward (nonlinear and tangent linear) computations, displacement vectors are extracted and applied to the 3d model fields as described by Nehrkorn et al. (2014). During the backward (adjoint) computation, the cost function gradient is computed with respect to the displacement vectors and stored in the  $u$ - and  $v$ -components of the gradient data structure. WRFDA makes use of a fully nonlinear outer loop and a linearized inner loop. Since this linearization makes the inner loop cost function quadratic, the conjugate gradient minimization algorithm that is used is efficient and has good convergence properties. After the inner loop minimization is complete, the resulting model field increments are output as the analysis increment. The full estimate of the analysis is then used in the next outer loop step (OLS) as the linearization point.

During the inner loop minimization, linearized versions of the displacements and observation operators are used to determine the incremental displacement. The full non-linear displacement algorithm is then applied in the outer loop to update the current estimate (*i.e.*, the analysis) of the 3d model fields, which serves as the linearization point for restarting the inner loop. In this way the displacements are calculated as a series of incremental displacements, which are effectively applied cumulatively at each OLS of the DAS.

#### *b. Background error covariance scaling and sensitivity testing*

We make the implicit assumption that the patterns in the displacement covariance statistics should be similar to that for horizontal wind vectors since it is the wind it-

self that is advecting the coherent features in the model fields. Then wind background error (units of m/s) covariances need to be rescaled for their application as displacement vector background errors (units of grid points) covariances. The effective parameters can be determined by running a simple single-observation test of the (standard) DAS. The effective background error standard deviation was determined to be approximately 2.7 m/s for the test case with default namelist settings for background error variance scaling (0.25). If used without rescaling, this would correspond to a displacement length scale in units of grid lengths (30 km in our test case), approximately 81 km. The standalone prototype used a displacement length scale of 150 km, so we multiply the standard variance rescaling by a factor of  $(150/81)^2$ . A similar procedure is used for the length-scale tuning. The single observation test revealed an effective e-folding length of the analysis increment of about 400-600 km, which is in rough agreement with the smallest scale allowed by the truncated spectral representation (total wavenumber 5) used by Grassotti et al. (1999).

The sensitivity of the DAS FCA solution to the size of the background error variance was examined by using both the rescaled (150 km) and unscaled (81 km) displacement length scale. The solution changed very little as a result. Similarly, providing either full radiosonde profiles (*i.e.*, surface pressure and wind, temperature, and humidity profiles), or just profiles of winds, had little effect on the solution. This is consistent with the findings of Nehrkorn et al. (2014) for this case. Their results were also not very sensitive to the tunable FCA parameters or whether IWV alone or IWV and surface pressure observations were used.

#### *c. Parallel processing considerations*

For applications to large domains that cannot be stored in memory available to a single compute node, the WRFDA FCA is implemented using MPI and halo exchanges, allowing the use of multiple cores within a given node or across nodes.<sup>5</sup> The native WRFDA domain decomposition is used to divide the domain into several patches to spread the load across multiple cores, where each core is assigned one patch. Complications arise when a displacement for the current grid point references a location outside the local patch.

When this occurs, separate MPI inter-process communication is used. Since the same set of displacement vectors is applied to multiple model fields (and levels),

<sup>5</sup>Each core is capable of executing one instance of a process or thread.

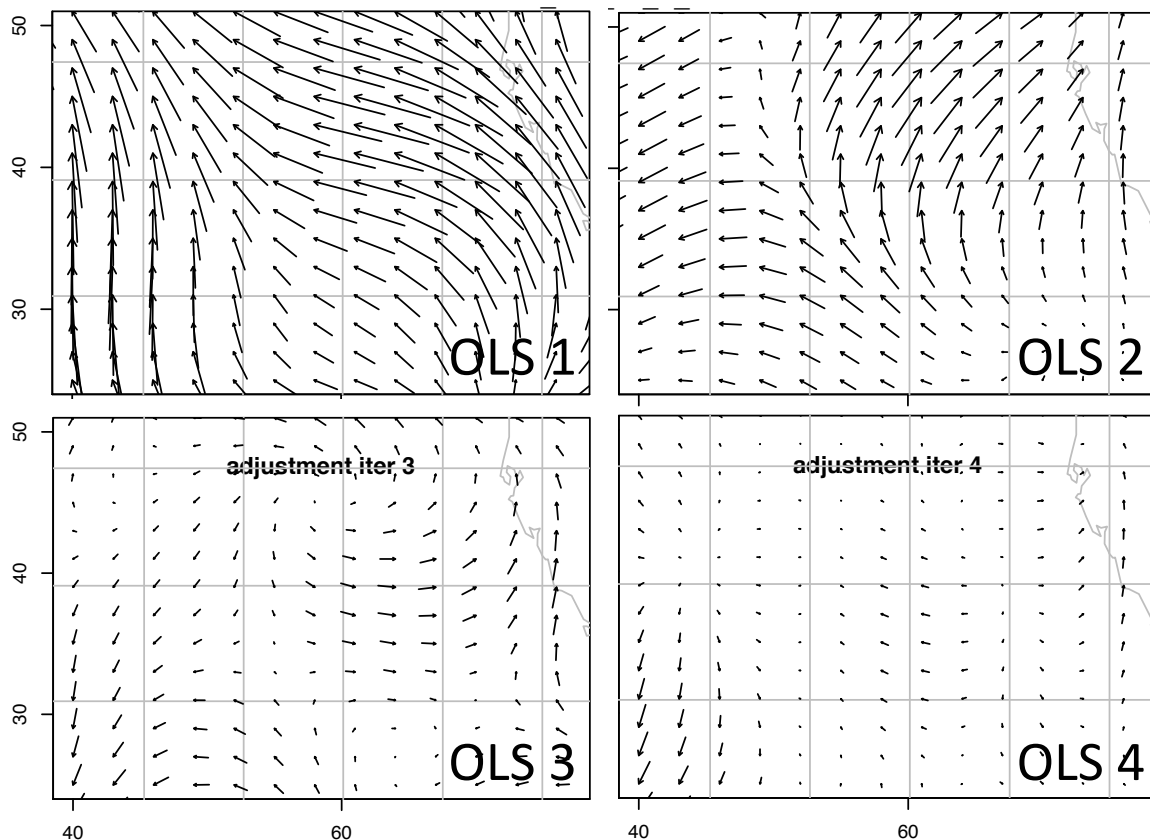


FIG. 5. The incremental displacements for the WRFDA FCA calculation of the Hurricane Katrina case from the first four OLSs. Displacements are shown as arrows pointing in the direction that the background field should be displaced, but are only plotted every third grid point in the  $x$ -direction and every other grid point in the  $y$ -direction for clarity.

the needed communication was organized into two steps such that information related to displacement vector origin and end points is exchanged only once. During the first step of this procedure, each process compiles a list of the displacement vectors with end points in its own patch of the model domain for which model values are needed at origin points outside its patch. The processes then exchange their list of needed points to create a global list of needed origin grid points. Each process searches the global list of needed points, and extracts two sets of information: (1) a set of displacement vectors with origin points inside its own patch; (2) a mapping of the previously determined needed origin points (outside its patch) to the global list of needed origin points. This information is then used in multiple applications of the second step, in which interpolated values at vector origin points are exchanged between processes. Finally, halo updates are called following the computation of displacements

analysis increments, so that updated halo values are available during the remainder of the DAS processing (e.g., for the computation of the innovation vector).

#### 4. Results

The OSSE setup of Section 2 is the same as in Nehr Korn et al. (2014), except that they used simulated IWV and/or surface pressure observations, and here we use simulated radiosonde observations. As we are assimilating RAOB soundings, we are limited to ingesting  $u$ ,  $v$ , temperature, and dew point. The WRFDA FCA prototype was run for ten OLSs to allow us to examine the convergence behavior.

We found that the WRFDA FCA solution converged after five or six OLSs (Fig. 4) with relatively small increments found after three OLSs (Fig. 5). After a small number of OLSs, little reduction in error was achieved. As is to be expected, the background cost function in-

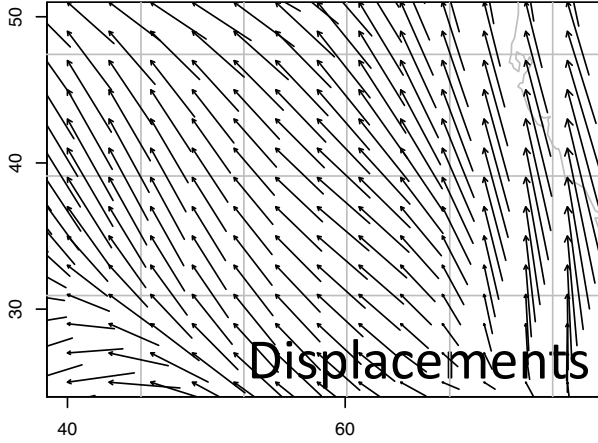


FIG. 6. WRFDA FCA-calculated displacements at 12 UTC, using simulated radiosonde observations. Plotted as in Fig. 5: Displacements are shown as arrows pointing in the direction that the background field should be displaced, but are only plotted every third grid point in the  $x$ -direction and every other grid point in the  $y$ -direction for clarity.

increases while the observation cost function decreases. Note that here  $J_b$  include displacements from all previous OLSs. In this case, the background cost function remains orders of magnitude smaller than the observation cost function, and the latter is indistinguishable from the total cost function on this plot. As the displacements are applied in the outer loop, each OLS produces its own incremental displacements (Fig. 5). The cumulative displacement vectors (shown below in Fig. 6) approximately correspond to the total displacement vectors applied to the background field. In that sense they are comparable to the vectors derived by Nehr Korn et al. (2014) using the Grassotti et al. (1999) methodology (shown in Fig. 9). The WRFDA FCA prototype displaces the vortex in the same way as found by Nehr Korn et al. (2014) during the first two OLSs, but shows some differences outside of the vortex that are largely introduced in subsequent OLSs. This level of agreement is remarkable given that the two methods use different observations (IWV vs. radiosondes) and different constraints.

Figure 7 shows the resulting IWV field after aligning the model state, and the error of the IWV field. Clearly the displacements are the correct direction and magnitude. The reconstructed IWV field has lost its symmetry—remember we are aligning the fields of potential temperature and relative humidity—but is nearly centered on the correct location. This asymmetry is seen both in the

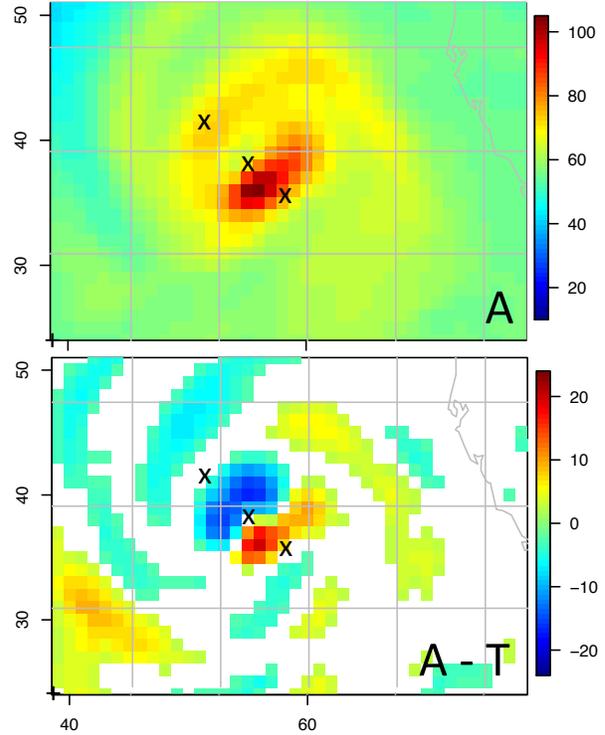


FIG. 7. WRFDA FCA adjusted IWV and IWV error at 12 UTC. Since the displacements are calculated from the simulated radiosonde observations and not IWV observations, the adjusted IWV field loses its symmetry. However, errors are reduced (compare to panel labeled B–T in Fig. 2).

IWV itself and in the IWV error. After a short-term forecast to 18 UTC, the IWV feature has regained its symmetry (Fig. 8) and is in the correct location. The forecast IWV errors ( $F_a-T$ ) are smaller and less organized than the aligned initial conditions IWV errors (A–T).

It is instructive to compare these results to the results of Nehr Korn et al. (2014). While there is agreement in the broad scale displacement fields, there are some interesting differences. Figure 9 shows the displacements determined by the standalone FCA using the IWV data. Note the generally similarity of the displacements in Fig. 6 and Fig. 9. Figure 10 shows the directly aligned IWV field, and its error ( $A^{IWV}-O$ , where  $O$  is the observations<sup>6</sup>). Here the IWV errors are very small—the FCA was applied to this field directly. Figure 11 is similar to Fig. 10—the displacements are identical—but here IWV is determined from the model fields that have

<sup>6</sup>Here  $O$  is used, not  $T$ . But  $O$  is subsampled  $T$ .

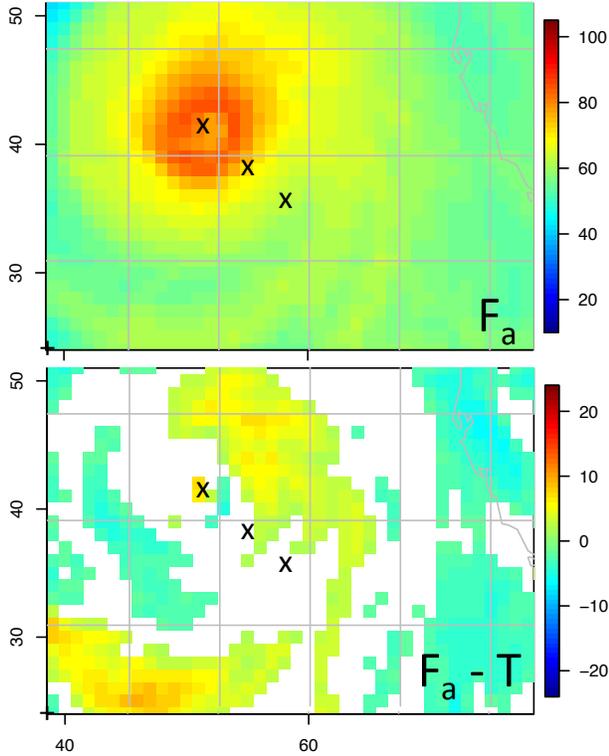


FIG. 8. The IWV WRFDA-adjusted forecast and forecast error at 18 UTC.

been aligned as described in Section 3. As was the case in Fig. 7, there is some loss of symmetry (but less here). The center of the IWV signature of the storm is displaced to the south and there is again a definite dipole structure in the errors. Again IWV regains a symmetrical structure after the short-term forecast (Fig. 12), but the IWV signature of the storm is forecast SSE of the truth, and this forecast is clearly inferior to that of Fig. 8.

## 5. Discussion and Conclusions

The feature calibration and alignment technique (FCA) is used to correct position errors in background fields. To do this, FCA determines 2d displacement vectors by solving the usual WRFDA variational data assimilation problem, but with the displacements as the control vector. The full model fields are then aligned following the generalization of the method of Hsiao et al. (2010) by Nehr Korn et al. (2014). This procedure minimizes dynamical imbalances by displacing conserved or quasi-conserved quantities and then recalculating needed derived quantities. Katrina OSSEs show the effectiveness

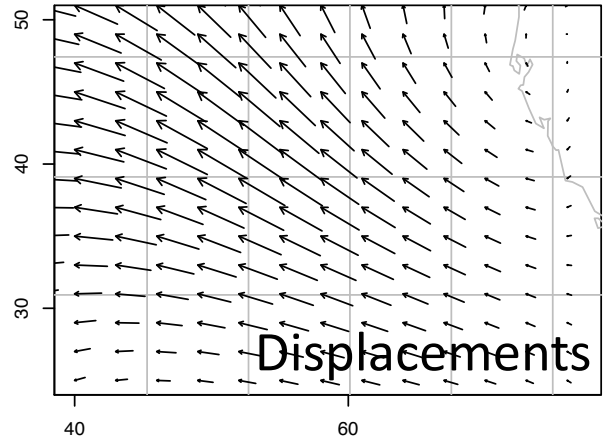


FIG. 9. Standalone FCA displacements calculated using IWV observations. Plotted as in Fig. 6.

of these procedures in correcting gross position errors and improving short-term forecasts.

Implementation of FCA into the quasi-operational WRF-DA represents a major advance over the standalone implementation of Nehr Korn et al. (2014). First, WRFDA FCA is not restricted to comparing 2d fields. Second, it can simultaneously make use of all observation types supported by WRFDA—no new observation operators are required. Third, the WRFDA estimation of error covariances can be used to refine the displacement error covariances. (In the current work, a simple rescaling of the wind background error covariances was used to characterize the displacement error covariances (Section 3.b).) Fourth, the parallel implementation of the WRFDA FCA algorithm is computationally efficient and scalable. By reducing demands on per-processor memory and overall wall-clock time it is feasible to apply the algorithm to large model domains and/or large numbers of cases. Fifth, the approach to implementing FCA in WRFDA could be applied to other variational data assimilation systems in a straightforward manner.

Comparison with the Katrina case identical twin OSSE of Nehr Korn et al. (2014) shows that the WRFDA FCA implementation performs properly and generally reproduces the major features of the standalone solutions. By design the standalone displacements greatly reduce the error in the aligned IWV field. In comparison, the alignment of the 3d model fields results in larger residual IWV errors, but these errors are still greatly reduced compared to the control case. When the aligned model fields are used as initial conditions in short-term forecasts, the forecasts of IWV are much improved relative to control, with

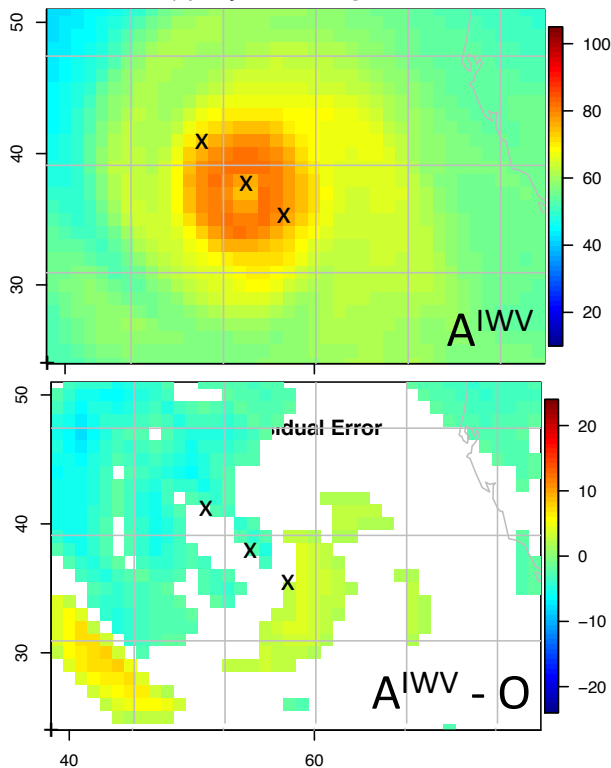


FIG. 10. Standalone FCA displacements of Fig. 9 applied directly to IWV. Plotted as in Fig. 7.

the greatest improvement seen in the WRFDA FCA experiment. This should be expected since the WRFDA FCA experiment used radiosonde profiles in place of IWV observations. The radiosonde data are superior in terms of quantity and diversity, represent the 3d structure of the atmosphere, and are more dynamically relevant than the IWV observations.

Future work will investigate various aspects of displacement increments, such as changes to the background error specification (beyond the basic rescaling exercised so far); the optimal combination of displacement and additive increments, and the selective use of different observation types for one or the other; the use of the principle of time continuity for the displacements; and the use of vertically varying displacement vectors.

#### Acknowledgments.

Funding for this work was provided by the US Air Force Weather Agency.

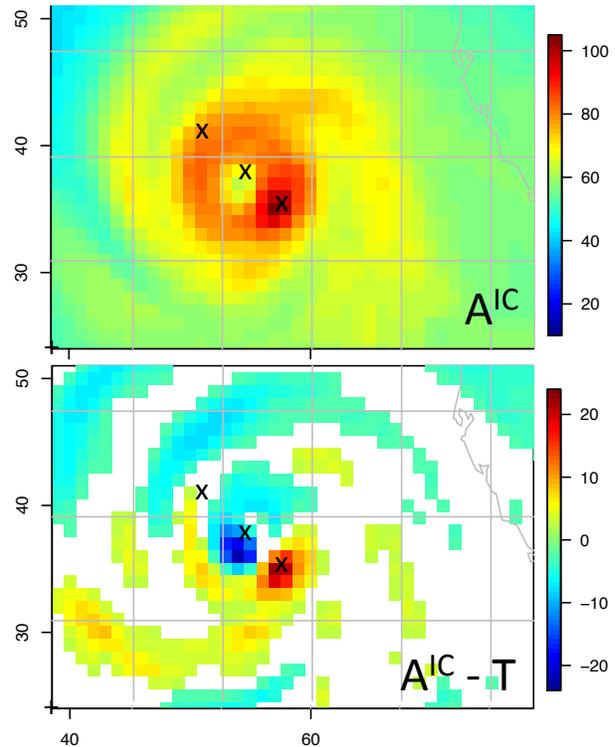


FIG. 11. Like Fig. 10, but here the IWV is calculated from the displaced model state using the FCA displacements of Fig. 9. The IWV field is more symmetric than in Fig. 7, but the magnitude of the errors are similar.

#### REFERENCES

- Ahijevych, D., E. Gilleland, B. G. Brown, and E. E. Ebert, 2009: Application of spatial verification methods to idealized and NWP-gridded precipitation forecasts. *Wea. Forecasting*, **24** (6), 1485–1497, doi:10.1175/2009WAF2222298.1.
- Barker, D., et al., 2012: The Weather Research and Forecasting model's community variational/ensemble data assimilation system: WRFDA. *Bull. Amer. Meteor. Soc.*, **93** (6), 831–843, doi:10.1175/BAMS-D-11-00167.1.
- Beezley, J. D. and J. Mandel, 2008: Morphing ensemble Kalman filters. *Tellus A*, **60** (1), 131–140, doi:10.1111/j.1600-0870.2007.00275.x.
- Brankart, J.-M., C.-E. Testut, D. Béal, M. Doron, C. Fontana, M. Meinville, P. Brasseur, and J. Veron, 2012: Towards an improved description of ocean

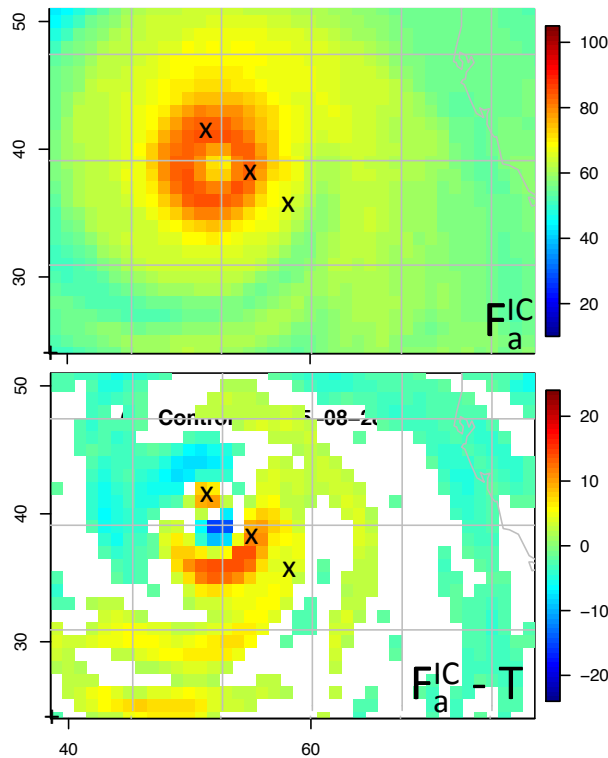


FIG. 12. The IWV of the standalone FCA-adjusted forecast ( $F_a^{IC}$ ) and forecast error ( $F_a^{IC}-T$ ) at 18 UTC.

uncertainties: effect of local anamorphic transformations on spatial correlations. *Ocean Sci.*, **8**, 121–142, doi:10.5194/os-8-121-2012.

Gay, D. M., 1990: Usage summary for selected optimization routines. Computing Science Technical Report No. 153, AT&T Bell Laboratories, Murray Hill, NJ.

Grassotti, C., H. Iskenderian, and R. N. Hoffman, 1999: Fusion of ground-based radar and satellite-based rainfall data using feature calibration and alignment. *J. Appl. Meteor.*, **38**, 677–695.

Hoffman, R. N., J. V. Ardizzone, S. M. Leidner, D. K. Smith, and R. M. Atlas, 2013: Error estimates for ocean surface winds: Applying Desroziers diagnostics to the cross-calibrated, multi-platform analysis of wind speed. *J. Atmos. Oceanic Technol.*, **30** (11), 2596–2603, doi:10.1175/JTECH-D-13-00018.1.

Hoffman, R. N. and C. Grassotti, 1996: A technique for assimilating SSM/I observations

of marine atmospheric storms. *J. Appl. Meteor.*, **35** (8), 1177–1188, doi:10.1175/1520-0450(1996)035<1177:ATFASO>2.0.CO;2.

Hoffman, R. N., Z. Liu, J.-F. Louis, and C. Grassotti, 1995: Distortion representation of forecast errors. *Mon. Wea. Rev.*, **123** (9), 2758–2770, doi:10.1175/1520-0493(1995)123<2758:DROFE>2.0.CO;2.

Hsiao, L.-F., et al., 2010: A vortex relocation scheme for tropical cyclone initialization in advanced research WRF. *Mon. Wea. Rev.*, **138** (8), 3298–3315, doi:10.1175/2010MWR3275.1.

Lawson, W. G. and J. A. Hansen, 2005: Alignment error models and ensemble-based data assimilation. *Mon. Wea. Rev.*, **133** (6), 1687–1709, doi:10.1175/MWR2945.1.

Michel, Y. and T. Auligné, 2010: Inhomogeneous background error modeling and estimation over Antarctica. *Mon. Wea. Rev.*, **138** (6), 2229–2252, doi:10.1175/2009MWR3139.1.

Nehrkorn, T., R. N. Hoffman, C. Grassotti, and J.-F. Louis, 2003: Feature calibration and alignment to represent model forecast errors: Empirical regularization. *Quart. J. Roy. Meteor. Soc.*, **129** (587), 195–218, doi:10.1256/qj.02.18.

Nehrkorn, T., B. Woods, T. Auligné, and R. N. Hoffman, 2014: Application of feature calibration and alignment to high-resolution analysis: Examples using observations sensitive to cloud and water vapor. *Mon. Wea. Rev.*, **142** (2), 686–702, doi:10.1175/MWR-D-13-00164.1.

Schöniger, A., W. Nowak, and H.-J. Hendricks Franssen, 2012: Parameter estimation by ensemble Kalman filters with transformed data: Approach and application to hydraulic tomography. *Water Resour. Res.*, **48**, W04 502, 18 pp. doi:10.1029/2011WR010462.

Simon, E. and L. Bertino, 2009: Application of the Gaussian anamorphosis to assimilation in a 3-D coupled physical-ecosystem model of the North Atlantic with the EnKF: A twin experiment. *Ocean Sci.*, **5**, 495–510, www.ocean-sci.net/5/495/2009/.

Wu, W.-S., R. J. Purser, and D. F. Parrish, 2002: Three-dimensional variational analysis with spatially inhomogeneous covariances. *Mon. Wea. Rev.*, **130** (12), 2905–2916.